IDA-PBC controller design for grid connected Front End Converters under non-ideal grid conditions

Federico M. Serra [a],*, Cristian H. De Angelo [b]

[a] Laboratorio de Control Automático (LCA), UNSL, Villa Mercedes, San Luis, Argentina
[b] Grupo de Electrónica Aplicada (GEA), UNRC, Río Cuarto, Córdoba, Argentina

ARTICLE INFO

ABSTRACT

A passivity-based non-linear controller design for three-phase front-end converters used to connect renewable energy sources to the grid is proposed in this paper. The control objective is to inject all the generated power to the grid, while adjusting the reactive power exchanged with the power system. Besides, generated currents must have very low distortion, in order to satisfy the standards, even when grid voltages are distorted or unbalanced. The proposed controller is first designed using the Interconnection and Damping Assignment strategy, which allows obtaining controller parameters while ensuring the closed-loop system stability. In order to ensure that the output currents have very low harmonic distortion, the obtained control laws are modified based on the fundamental positive sequence grid voltage, obtained from a positive sequence detector. The proposal allows controlling both injected powers and DC-link voltage, from a unique controller design. Simulation and experimental results are presented to validate the proposed controller.

© 2016 Elsevier B.V. All rights reserved.

1. Introduction

The use of power electronic converters to connect renewable energy sources to the electric grid has undergone significant development in recent decades [1,2]. These converters allow flexible and efficient connection between the generation system and the grid, resulting in an important research area in which the control of these converters are concerned [3,4]. In particular the converter that performs interconnection with the grid is known as active Front End Converter (FEC) and generally consists of a Voltage Source Converter (VSC) and an output filter in order to reduce the injected currents ripple (Fig. 1). In these systems, the amplitude and frequency of the voltage at the coupling point are imposed by the grid. Then, the control objectives for the FEC are to inject all of the power available on the DC side to the grid and control the reactive power exchanged with the power system. To achieve these objectives, it is necessary that the FEC synchronizes with the angle of the grid voltage while the waveform of the injected currents must also be controlled. Such currents must be almost sinusoidal, with harmonic content below the limits imposed by the standards. Standard IEEE-1547 [5] establish that the maximum total harmonic distortion (THD) for the current injected by distributed resources must

be below 5%. Besides, this standard sets limits to the amplitude of each harmonic, tolerating a maximum amplitude of 5% each.

If the mains voltage is pure sinusoidal and balanced, and the input DC current is constant, generating sinusoidal output currents (with low harmonic content which does not exceed the values set by the standards) can be achieved by simple strategies such as current control in *dq* coordinates [6,7]. A better dynamic performance can be achieved when using more complex strategies, which include nonlinear control techniques [8,9]. However, these strategies do not give satisfactory results if the mains voltage is unbalanced, with harmonic distortion and/or the input current has a significant ripple.

In these cases, special control strategies must be designed to generate adequate currents. These control strategies allow the generation of sinusoidal currents at the expense of allowing oscillation in the DC-link voltage, being possible to control only the average value of such voltage. This oscillation in the DC-link voltage occurs because the system has to maintain the power balance between the input and output of the converter.

Control schemes for a grid-connected VSC considering unbalanced voltages are presented in [10,11]. In Yazdani and Iravani [10], two different control objectives are proposed: one tries to balance the line currents controlling only the average value of the DC-link voltage, while the second allows to mitigate the ripple of the DC-link voltage produced due to the imbalance in the grid voltage, but this implies that the injected currents are unbalanced. In this
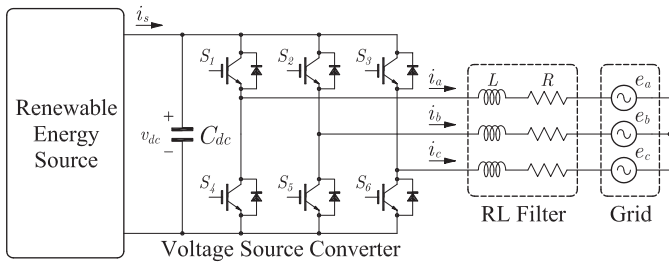
Fig. 1. FEC connected to the grid.

case, sinusoidal currents generation requires decomposition of the system into two subsystems, a positive sequence system and a negative sequence one. Then, a particular controller must be designed for each subsystem [11].

An attempt to avoid schemes with control loops for each sequence component is to use Direct Power Control (DPC) strategies [12–14]. A VSC control using DPC is proposed in Eloy-Garcia et al. [12], in order to achieve symmetrical currents when the voltage is unbalanced. In Shang et al. [13], an improved DPC control method for obtaining symmetric and sinusoidal grid currents, or to eliminate the ripple on the active and reactive powers, is presented. These approaches allow to directly regulate active and reactive powers without taking into account the negative sequence components of voltages and currents. This strategy is improved in Xiao et al. [14], in order to eliminate the DC voltage ripple, and to obtain a constant switching frequency. However, in all these cases, the effect of harmonic distortion in the grid voltage is not considered.

For the case in which grid voltage includes unbalance and distortion, Nguyen et al. [15], tries to solve this problem using a multi-loop current controller that regulates positive-sequence currents, negative-sequence currents and fifth and seventh harmonic, separately, using PI and resonant controllers. A combination of PI and a bank of resonant controllers is also proposed in Trinh and Lee [16]. In Jang and Lee [17], a high performance control scheme is proposed in order to reduce harmonics in the grid current and decrease the DC-link voltage ripple. However, as in Yazdani and Iravani [10] the above methods require implementing a reference frame rotation and a specific controller for each harmonic current to be controlled, plus an additional controller for the DC voltage, thus resulting in computational intensive implementations. To cope this problem, stationary reference-frame proportional-resonant controllers are proposed in Lee et al. [18], while predictive current control is presented in Hu et al. [19]. However, tuning of each control loop is still an issue in these proposals. Furthermore, none of the above cases considered distortion in the DC side current.

In this paper a controller for a grid-connected FEC is proposed using the passivity-based control strategy known as Interconnection and Damping Assignment (IDA) [20,21]. This design methodology was chosen because it is an energy-based control strategy, which allows to give physical interpretation to the control action and to define clearly the conditions for ensuring closed-loop stability. The controller design, following the steps of the IDA strategy, is an organized design using matrix equations, where each of these matrices has a well defined physical meaning. Thus, the designer can modify the structure of the system for simplicity, and thus solve the problem of having more variables than control actions. Also, this methodology simplifies the determination of the parameters of the controller.

The main control objective is to inject all of the available power on the DC side to the grid and control the reactive power exchanged with the power system, while ensuring that the current injected into the grid be practically sinusoidal, with harmonic content below the values imposed by the standards. When the voltage is pure

sinusoidal and balanced, the latter can be achieved by using an IDA controller as proposed by the authors in Serra et al. [8]. However, if the mains voltage is unbalanced and distorted, and the input current is not constant, such strategy does not allows to eliminate the distortion of the injected currents.

Therefore, we propose a modification to the controller presented in Serra et al. [8] to compensate for distortions and unbalance of the mains voltage and the input current. With this modification we achieve a very low distortion of the current injected to the grid, independently of the mains voltage distortion and the ripple of the DC input current. First, control laws are obtained using IDA strategy, based on the selection of the closed-loop energy function in order to ensure system stability. Then, these laws are modified using the information of the fundamental component of the positive sequence voltage, obtained by a positive sequence detector which provides information about angle and amplitude of this component.

The obtained control laws allow relating the state variables of the system in order to obtain an equation to control the DC-link voltage through the direct axis current, thus enabling the injection of all generated power to the grid, but ensuring that the distortion of the injected current is within the allowable values for the standards. Moreover, the quadrature axis current is used to control the reactive power exchanged with the power system.

Simulation and experimental results obtained on a laboratory prototype are presented in order to validate the proposed controller and the implementation of IDA strategy for this kind of systems, which has not yet been presented in the literature.

2. Front End Converter model

The Front End Converter consists of a three-phase universal bridge-reversible PWM Voltage Source Converter (VSC) with Isolated Gate Bipolar Transistor (IGBT) (S_1, ..., S_6) and an RL output filter, as shown in Fig. 1. Current i_s comes from the generation side converter and the grid is modeled using three voltage sources e_a, e_b and e_c.

In order to design a controller for the FEC using the IDA strategy, it must be represented as a port-Hamiltonian (pH) system,

$$\dot{\mathbf{x}} = [\mathbf{J}(\mathbf{x}, \mathbf{u}) - \mathbf{R}(\mathbf{x})]\frac{\partial H(\mathbf{x})}{\partial \mathbf{x}} + \mathbf{g}(\mathbf{x}, \mathbf{u})\mathbf{e}, \tag{1}$$

$$\mathbf{y} = \mathbf{g}^T(\mathbf{x}, \mathbf{u})\frac{\partial H(\mathbf{x})}{\partial \mathbf{x}}, \tag{2}$$

where $\mathbf{x}$ is the state vector (energy variables), $\mathbf{u}$ is the control vector, $H(\mathbf{x})$ is the system energy function, $\mathbf{g}(\mathbf{x}, \mathbf{u})$ is the port matrix, $\mathbf{e}$ is the vector of external sources, $\mathbf{y}$ is the port output vector, $\mathbf{J}(\mathbf{x}, \mathbf{u}) = -\mathbf{J}^T(\mathbf{x}, \mathbf{u})$ is the anti-symetric interconnection matrix and $\mathbf{R}(\mathbf{x}) = \mathbf{R}^T(\mathbf{x}) \geq 0$ is the symmetric positive semi-definite damping matrix. The interconnection matrix represents the internal energy flow while the damping matrix represents the system dissipation.

The total stored energy function, $H(\mathbf{x})$, is given by the sum of the energy stored in the filter inductances and in the DC-link capacitor,

$$H(\mathbf{x}) = \frac{Li_d^2}{2} + \frac{Li_q^2}{2} + \frac{C_{dc}v_{dc}^2}{2}, \tag{3}$$

Then, the pH model of the FEC can be expressed as follows [8],

$$\begin{bmatrix} L\dot{i}_d \\ L\dot{i}_q \\ C_{dc}\dot{v}_{dc} \end{bmatrix} = \begin{bmatrix} -R & -\omega_{dq}L & m_d \\ \omega_{dq}L & -R & m_q \\ -m_d & -m_q & 0 \end{bmatrix} \begin{bmatrix} i_d \\ i_q \\ v_{dc} \end{bmatrix} + \begin{bmatrix} 1 & 0 & 0 \\ 0 & 1 & 0 \\ 0 & 0 & 1 \end{bmatrix} \begin{bmatrix} -e_d \\ -e_q \\ i_s \end{bmatrix} \tag{4}$$

where ω_{dq} is the angular speed of the reference frame, which in this case coincides with the grid frequency; i_d and i_q are the currents in

the dq reference frame, obtained through the transformation of i_a, i_b and i_c; e_d and e_q are the grid voltages obtained through the transformation of e_a, e_b and e_c; m_d and m_q are the modulation indexes, C_{dc} is the DC-link capacitance; L and R are the inductance and resistance of the output filter, respectively.

For this system, the interconnection and damping matrices are,

$$\mathbf{J}(\mathbf{u}) = \begin{bmatrix} 0 & -\omega_{dq}L & m_d \\ \omega_{dq}L & 0 & m_q \\ -m_d & -m_q & 0 \end{bmatrix}, \qquad \mathbf{R} = \begin{bmatrix} R & 0 & 0 \\ 0 & R & 0 \\ 0 & 0 & 0 \end{bmatrix}. \tag{5}$$

3. Controller design

The proposed control strategy mainly aims to inject all of the available power on the DC side to the grid and control the reactive power exchanged with the power system, further ensuring that the current injected to the grid complies with the standards. The objective of injecting all available active power to the grid can be achieved by maintaining the DC-link voltage constant. This voltage control can be performed with the control of the direct current, i_d, through the design method described below. Moreover, the reactive power control can be done directly by controlling the quadrature current, i_q.

Therefore, the design of the controller consist on ensuring that the state variables of the system (1) reach the reference vector,

$$\mathbf{x}^* = \begin{bmatrix} Li_d^* & Li_q^* & C_{dc}v_{dc}^* \end{bmatrix}^T. \tag{6}$$

To this end, we propose a control law $\mathbf{u} = \beta(\mathbf{x})$, such that the dynamics of the closed-loop system can be described by a pH system of the form [20],

$$\dot{\mathbf{x}} = [\mathbf{J}_d(\mathbf{x}, \mathbf{u}) - \mathbf{R}_d(\mathbf{x})] \frac{\partial H_d(\mathbf{x})}{\partial \mathbf{x}}, \tag{7}$$

such that $\mathbf{x}^*$ be a minimum of $H_d(\mathbf{x})$,

$$\left. \frac{\partial H_d(\mathbf{x})}{\partial \mathbf{x}} \right|_{\mathbf{x} = \mathbf{x}^*} = 0, \qquad \left. \frac{\partial^2 H_d(\mathbf{x})}{\partial \mathbf{x}^2} \right|_{\mathbf{x} = \mathbf{x}^*} > 0, \tag{8}$$

where $H_d(\mathbf{x})$ is the desired energy function for the closed-loop system, and $\mathbf{J}_d(\mathbf{x}, \mathbf{u})$ and $\mathbf{R}_d(\mathbf{x})$ are the desired interconnection and damping matrices, which can be described as follows,

$$\mathbf{J}_d(\mathbf{x}, \mathbf{u}) = \mathbf{J}(\mathbf{x}, \mathbf{u}) + \mathbf{J}_a(\mathbf{x}, \mathbf{u}), \tag{9}$$

$$\mathbf{R}_d(\mathbf{x}) = \mathbf{R}(\mathbf{x}) + \mathbf{R}_a(\mathbf{x}). \tag{10}$$

Matrices $\mathbf{J}_a(\mathbf{x}, \mathbf{u})$ and $\mathbf{R}_a(\mathbf{x})$ are used to synthesize the proposed control strategy. $\mathbf{R}_a(\mathbf{x})$ is the matrix that represents the damping that must be added to the system in order to achieve the asymptotic stability of the control error. On the other hand, $\mathbf{J}_a(\mathbf{x}, \mathbf{u})$ is a matrix that allows changing the internal relationship between state variables (interconnection) in order to obtain the desired error dynamics, which in turn allows an easier determination of controller parameters. Besides, in this case, the choice of $\mathbf{J}_a(\mathbf{x}, \mathbf{u})$ plays an important role in solving the problem of having more control variables than control actions.

From the Proposition 1 of [20], given $\mathbf{J}(\mathbf{x}, \mathbf{u})$, $\mathbf{R}(\mathbf{x})$, $H(\mathbf{x})$, $\mathbf{g}(\mathbf{x}, \mathbf{u})$, if we can find functions $\beta(\mathbf{x})$, $\mathbf{J}_a(\mathbf{x}, \mathbf{u})$, $\mathbf{R}_a(\mathbf{x})$, and a vector function $K(\mathbf{x})$ satisfying,

$$\left[\mathbf{J}(\mathbf{x}, \beta(\mathbf{x})) + \mathbf{J}_a(\mathbf{x}, \beta(\mathbf{x})) - (\mathbf{R}(\mathbf{x}) + \mathbf{R}_a(\mathbf{x})) \right] K(\mathbf{x})$$

$$= -\left[\mathbf{J}_a(\mathbf{x}, \beta(\mathbf{x})) - \mathbf{R}_a(\mathbf{x}) \right] \frac{\partial H(\mathbf{x})}{\partial \mathbf{x}} + \mathbf{g}(\mathbf{x}, \beta(\mathbf{x}))\mathbf{e}, \tag{11}$$

and such that,

• Structure preservation,

$$\mathbf{J}_d(\mathbf{x}, \mathbf{u}) := \mathbf{J}(\mathbf{x}, \mathbf{u}) + \mathbf{J}_a(\mathbf{x}, \mathbf{u}) = -[\mathbf{J}(\mathbf{x}, \mathbf{u}) + \mathbf{J}_a(\mathbf{x}, \mathbf{u})]^T, \tag{12}$$

$$\mathbf{R}_d(\mathbf{x}) := \mathbf{R}(\mathbf{x}) + \mathbf{R}_a(\mathbf{x}) = [\mathbf{R}(\mathbf{x}) + \mathbf{R}_a(\mathbf{x})]^T \geq 0. \tag{13}$$

• Integrability,

$$\frac{\partial K(\mathbf{x})}{\partial \mathbf{x}} = \left[\frac{\partial K(\mathbf{x})}{\partial \mathbf{x}} \right]^T. \tag{14}$$

• Equilibrium assignment,

$$K(\mathbf{x}^*) = -\frac{\partial H(\mathbf{x}^*)}{\partial \mathbf{x}}. \tag{15}$$

• Lyapunov stability,

$$\frac{\partial K(\mathbf{x}^*)}{\partial \mathbf{x}} > -\frac{\partial^2 H(\mathbf{x}^*)}{\partial \mathbf{x}^2}. \tag{16}$$

the closed-loop system (7) will be a pH system where,

$$H_d(\mathbf{x}) := H(\mathbf{x}) + H_a(\mathbf{x}), \tag{17}$$

and,

$$\frac{\partial H_a(\mathbf{x})}{\partial \mathbf{x}} := K(\mathbf{x}). \tag{18}$$

Furthermore, $\mathbf{x}^*$, will be a (locally) stable equilibrium of the closed-loop system. From this proposition, it can be appreciated that the key for the design procedure relies on solving (11). There are numerous methods to solve this equation, as shown in Ortega and Garcia-Canseco [21]. In this paper, the "Algebraic IDA" method is used, which consist on first choosing the desired energy function $H_d(\mathbf{x})$ for the closed-loop system. Then, (11) results an algebraic equation in terms of $\mathbf{J}_d(\mathbf{x}, \mathbf{u})$ and $\mathbf{R}_d(\mathbf{x})$, which can be choosen taking into account the restrictions imposed to achieve the closed-loop stability.

In order to make the system states ($\mathbf{x}$) tends to its reference value ($\mathbf{x}^*$) asymptotically, $H_d(\mathbf{x})$ is chosen as a Lyapunov function,

$$H_d(\mathbf{x}) = \frac{1}{2}(\boldsymbol{\epsilon}^T \mathbf{P}^{-1} \boldsymbol{\epsilon}), \tag{19}$$

such that (8) is fulfilled.

In (19), $\boldsymbol{\epsilon} = \mathbf{x} - \mathbf{x}^*$, and,

$$\mathbf{P} = \begin{bmatrix} L & 0 & 0 \\ 0 & L & 0 \\ 0 & 0 & C_{dc} \end{bmatrix}, \tag{20}$$

Time derivative of $H_d(\mathbf{x})$ is,

$$\dot{H}_d(\mathbf{x}) = -\boldsymbol{\epsilon}^T \mathbf{P}^{-1} \mathbf{R}_d \mathbf{P}^{-1} \boldsymbol{\epsilon} < 0, \tag{21}$$

therefore, $\mathbf{R}_d(\mathbf{x})$ must be a positive definite matrix in order to guarantee the error convergence to zero, which determines the choice of the elements of $\mathbf{R}_a(\mathbf{x})$. In this work, matrix $\mathbf{R}_a(\mathbf{x})$ is chosen as,

$$\mathbf{R}_a = \begin{bmatrix} R_1 & 0 & 0 \\ 0 & R_2 & 0 \\ 0 & 0 & R_3 \end{bmatrix}, \tag{22}$$

with R_1, R_2 and R_3 greater than zero.

The elements of $\mathbf{J}_a(\mathbf{x}, \mathbf{u})$ can be selected with the aim of canceling the undesired coupling between some state variables, while maintaining coupled those variables which allows to deal with systems

Table 1
Controller parameters.

Parameter	Value
R_1	$7.4\,\Omega$
R_2	$7.4\,\Omega$
R_3	$0.94\,\Omega^{-1}$

with more control variables than control actions [22]. In this case $\mathbf{J}_a(\mathbf{x}, \mathbf{u})$ is chosen as follows:

$$\mathbf{J}_a(\mathbf{u}) = \begin{bmatrix} 0 & \omega_{dq}L & -m_d \\ -\omega_{dq}L & 0 & -m_q \\ m_d & m_q & 0 \end{bmatrix}. \tag{23}$$

Using (11), (12) and (17), the partial-differential equation for the FEC is,

$$\left[\mathbf{J}(\beta(\mathbf{x})) - \mathbf{R}\right]\frac{\partial H_a(\mathbf{x})}{\partial \mathbf{x}} = -\left[\mathbf{J}_a(\beta(\mathbf{x})) - \mathbf{R}_a\right]\frac{\partial H_d(\mathbf{x})}{\partial \mathbf{x}} + \mathbf{g}e, \tag{24}$$

which can be solved to obtain the control laws,

$$m_d = \frac{Ri_d^* + \omega_{dq}Li_q - R_1(i_d - i_d^*) + e_d}{v_{dc}}, \tag{25}$$

$$m_q = \frac{Ri_q^* - \omega_{dq}Li_d - R_2(i_q - i_q^*) + e_q}{v_{dc}}. \tag{26}$$

Besides, i_d^* can be obtained from (24) and (4) considering $i_d = i_d^*$, $i_q = i_q^*$ and $e_q = 0$,

$$i_d^* = \frac{1}{2}\left[-\frac{e_d}{R} \pm \sqrt{\left(\frac{e_d}{R}\right)^2 + \frac{\Delta}{R} - 4i_q^{*2}}\right], \tag{27}$$

with,

$$\Delta = 4v_{dc}[i_s + R_3(v_{dc} - v_{dc}^*)]. \tag{28}$$

With this controller, the error dynamics results in,

$$\dot{\epsilon}_{i_d} = -\frac{(R + R_1)}{L}\epsilon_{i_d}, \tag{29}$$

$$\dot{\epsilon}_{i_q} = -\frac{(R + R_2)}{L}\epsilon_{i_q}, \tag{30}$$

$$\dot{\epsilon}_{v_{dc}} = -\frac{R_3}{C_{dc}}\epsilon_{v_{dc}}, \tag{31}$$

where it can be seen that the closed-loop system results stable, with asymptotic convergence of the error to zero. It must also be noted that (29) - (31) is a linear system where error dynamics are decoupled. Thus, this system can be easily solved for the values of R_1, R_2 and R_3 in order to obtain the desired convergence speed for each error. The values of R_1, R_2 and R_3 used for obtaining the experimental results are included in Table 1.

For the obtained controller, the components of the reference vector, $\mathbf{x}^*$, can be chosen as follows: the reference of the DC-link voltage must be set constant ($v_{dc}^* = \text{const.}$) in order to inject all the generated power into the grid; i_d^* can be calculated from (27); and i_q^* can be obtained from the reactive power that must be exchanged with the power system taking into account that this power is proportional to the i_q current ($q = i_d e_q - i_q e_d \rightarrow q = -i_q e_d$ due to $e_q = 0$).

3.1. Non-ideal grid voltage and converter input current

The controller design presented above allows sinusoidal current injection to the grid whenever the voltage is pure sinusoidal and balanced, and the input current, i_s, be a pure DC. In practice, the grid voltage usually presents some degree of unbalance and harmonics, and also the converter input current could contain a significant
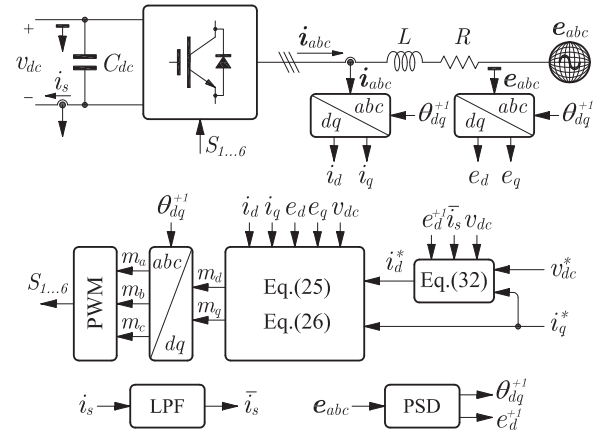

Fig. 2. Proposed passivity-based control strategy.

ripple due a rectification stage, so it is not possible to ensure that the injected currents are sinusoidal, complying with international standards.

To achieve the currents injected by the inverter have low distortion, the original controller, described by (25)–(27) is modified as follows. First, the reference frame used in the design of the controller is oriented to the angle determined by the fundamental component of the positive-sequence voltage (θ^{+1}), instead of directly using the angle calculated with the measured voltages. Besides, the fundamental component of the positive-sequence voltage (e_d^{+1}) and the mean value of the input current ($\bar{i}_s$) are used in the calculation of i_d^*.

Then, Park's transformation used to determine the components of (25) and (26) are calculated using (θ^{+1}), while i_d^* is calculated as follows:

$$i_d^* = \frac{1}{2}\left[-\frac{e_d^{+1}}{R} \pm \sqrt{\left(\frac{e_d^{+1}}{R}\right)^2 + \frac{\Delta^{+1}}{R} - 4i_q^{*2}}\right], \tag{32}$$

where,

$$\Delta^{+1} = 4v_{dc}[\bar{i}_s + R_3(v_{dc} - v_{dc}^*)]. \tag{33}$$

In this way we obtain sinusoidal current injected to the grid in compliance with the standards, when the supply voltage is distorted and the input current is not a pure DC. This results in an oscillating power injected to the grid, thus being only possible to control the average value of the DC-link voltage.

Fig. 2 shows a block diagram of the proposed control strategy, where it can be appreciated that a Low Pass Filter (LPF) was used to obtain the mean value of the input current $\bar{i}_s$. A Positive-Sequence Detector (PSD) is utilized to obtain the angle and amplitude of the fundamental component of the positive-sequence grid voltage. The implemented PSD is a DSOGI-FLL, which has a better performance with respect to other PSDs when grid voltage is unbalanced and distorted [23].

4. Results

In order to evaluate the performance of the proposed controller for the FEC against different operating conditions, simulation and experimental tests were performed.

4.1. Simulation results

Simulation results were obtained using SimPowerSystem from Matlab. For these results, voltage unbalance and harmonic distortion greater than those obtained in the experiments were
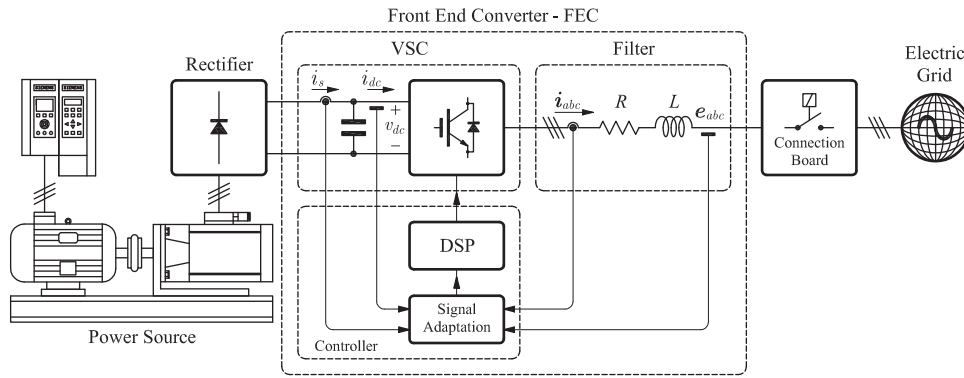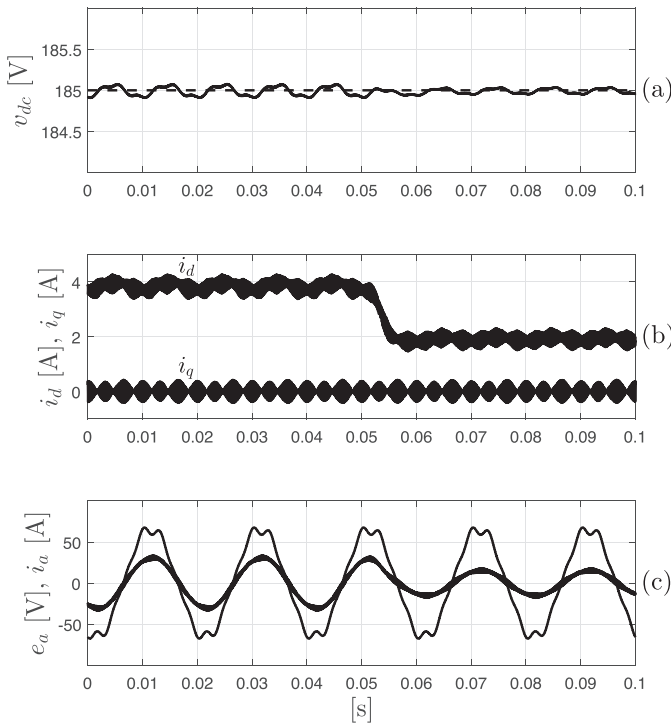
Fig. 3. Block diagram of the experimental prototype.

Fig. 4. Performance of the proposed IDA controller: (a) DC-link voltage; (b) d and q axis currents; (c) current and voltage at phase a (simulation results).

Table 2
FEC and grid parameters.

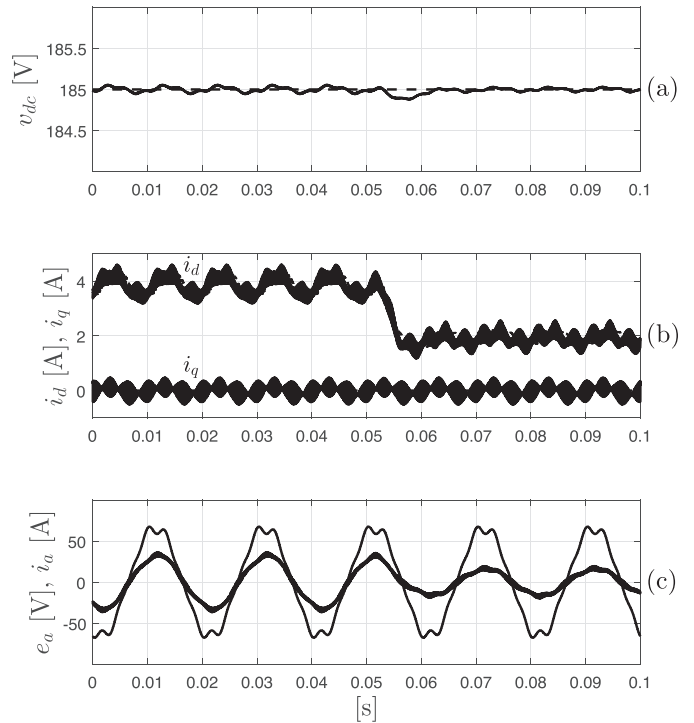| Parameter	Value
L	4 mH
R	0.2 Ω
C	4700 μF
$R_{on_{(IGBT)}}$	2.6 mΩ
f_s	10 kHz
e_a, e_b, e_c	73.5 V
f	50 Hz

Fig. 5. Performance of the classic PI controller: (a) DC-link voltage; (b) d and q axis currents; (c) current and voltage at phase a (simulation results).

considered, in order to test the proposed strategy under more unfavorable conditions. In this case, a 5% of fifth and seventh harmonics and a 10% voltage unbalance condition (calculated according to IEC standard) was simulated.

Figs. 4–7 present a comparison of the behavior of the proposed strategy with a classic controller, implemented using PI controllers in decoupled d and q axis. Parameters of the IDA controller are those shown in Table 1, while the PI controllers were adjusted so as to obtain a time response similar to the proposed controller. The FEC and grid parameters are presented in Table 2.

Behavior of the proposed IDA controller is shown in Fig. 4, while Fig. 5 presents the results of the classic controller. As can be seen in Figs. 4(a) and 5(a), both controllers allow regulating the mean value of the DC-link voltage, independently of the changes on the input power. Besides, in both cases the ripple of the DC-link voltage remains between acceptable limits. However, the classic controller shows a more noticeable transient when the input power changes.

Figs. 4(b) and 5(b) show the currents in the d and q axis for both control strategies. As can be appreciated, the proposed IDA controller produce currents with lower distortion, which is reflected

in the output current shown in Fig. 4(c). In spite of the high voltage distortion and unbalance, the proposed controller allows injecting a sinusoidal current, with lower distortion than the one produced with the classic controller, shown in Fig. 5(c).

The latter is better appreciated in the frequency spectra of the output currents, shown in Figs. 6 and 7 for the proposed controller and the classic one, respectively. As can be seen, the harmonic content is lower with the proposed strategy (THD 1.9%) than the obtained with the classic controller (THD 6.1%). In this case, the
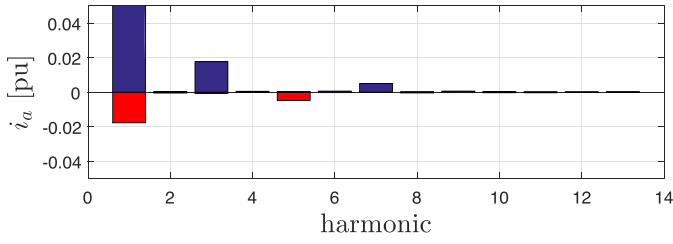
Fig. 6. Frequency spectrum of grid current with the proposed IDA controller (simulation result).
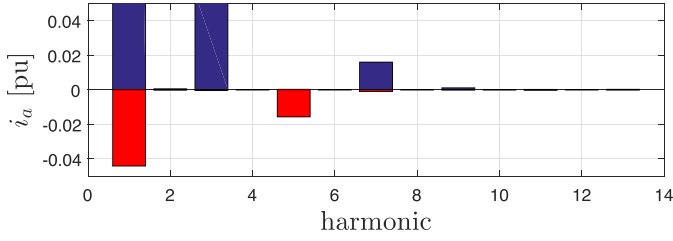

Fig. 7. Frequency spectrum of grid current with the classic PI controller (simulation result).

Table 3
SIEMENS 3ph-Brushless Servomotor 1FT6084-8AF71-3TH0-Z.

Parameter	Value
I_0	11.3/14 A
V_{in}	270 V Y
M_n	14.7 Nm
N	3000 RPM

distortion for the PI-based controller is beyond the allowed by standards.

4.2. Experimental results

The implemented prototype consists of the FEC, comprising a VSC built with 1200 V – 75 A Semikron IGBT (SKM75GB124D) plus an RL filter which allows connecting the VSC to the grid. A step-up transformer was also used in order to adapt voltage levels between converter output and the grid. The control strategy for the FEC was implemented on a Texas Instruments floating point DSP (TMS320F28335). Parameters of the FEC and network match those shown in Table 2. We used a sinusoidal PWM with 10 kHz switching frequency and 185 V DC-link. As a power source a permanent magnet synchronous generator (SIEMENS 3-Brushless Servomotor 1FT6084-8AF71-3TH0-Z) was used. Generator data are shown in Table 3. A three-phase induction motor which is driven by a variable speed drive, was coupled to the generator, thus emulating the behavior of a wind generation system. Fig. 3 shows a block diagram of the experimental prototype.

4.2.1. Algorithm
The proposed control algorithm is implemented in the DSP at a 100 μs sample interruption. The implemented algorithm can be summarized as follows:

- Signals acquisition and conditioning. Measured variables are i_s, v_{dc}, i_a, i_b, e_a, and e_b. Since the converter is connected to a three-wire system, only two line currents and system voltages are measured. Then, the remaining currents and voltages are obtained from $i_c = -i_a - i_b$ and $e_c = -e_a - e_b$, respectively. Measured input current is processed by a LPF to obtain $\bar{i}_s$.
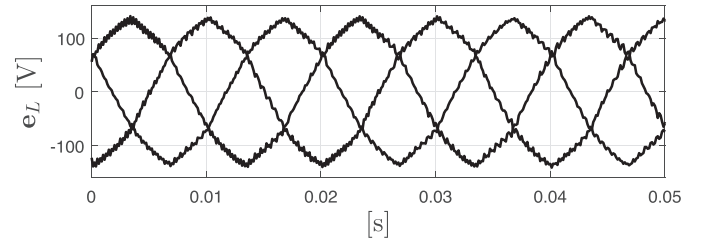

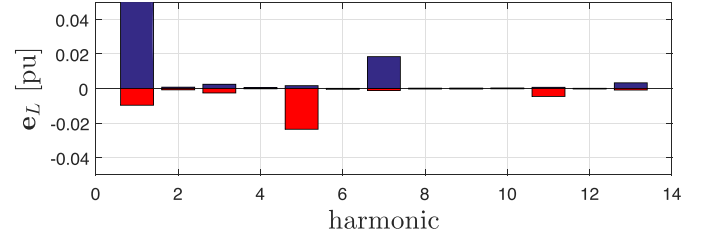**Fig. 8.** Line to line grid voltage (experimental result).

Fig. 9. Frequency spectrum of grid voltage (experimental result).

- Calculation of the fundamental positive-sequence component of the grid voltage ($\mathbf{e}_{abc}^{+1}$) using a DSOGI-FLL PSD implemented in the same DSP (see [24]).
- Park's transformation of the measured variables:

$$\mathbf{i}_{abc} \longrightarrow \mathbf{i}_{dq},$$
$$\mathbf{e}_{abc} \longrightarrow \mathbf{e}_{dq},$$
$$\mathbf{e}_{abc}^{+1} \longrightarrow \mathbf{e}_{dq}^{+1}.$$

- Calculation of the modulation indexes from the reference values i_q^* and v_{dc}^*:

$$i_d^* = \frac{1}{2}\left[-\frac{e_d^{+1}}{R} \pm \sqrt{\left(\frac{e_d^{+1}}{R}\right)^2 + \frac{\Delta^{+1}}{R} - 4i_q^{*2}} \right],$$

$$\Delta^{+1} = 4v_{dc}\left[\bar{i}_s + R_3\left(v_{dc} - v_{dc}^*\right)\right].$$

$$m_d = \frac{Ri_d^* + \omega_{dq}Li_q - R_1(i_d - i_d^*) + e_d}{v_{dc}},$$

$$m_q = \frac{Ri_q^* - \omega_{dq}Li_d - R_2(i_q - i_q^*) + e_q}{v_{dc}}.$$

- Inverse Park's transformation of the modulation indexes:

$$\mathbf{m}_{dq} \longrightarrow \mathbf{m}_{abc}.$$

- Update of the PWM registry values.

4.2.2. Experimental tests
Fig. 8 shows the measured (line-line) grid voltage, and Fig. 9 shows its frequency spectrum. It can be seen that voltage has about 2% of 5th and 7th harmonics. It also presents a 1% of unbalance (measured according to IEC). This distortion in the grid voltage is enough to prove experimentally the performance of the control strategy proposed in this paper. Fig. 10 shows the voltage and current at phase a for a test consisting on delivering constant
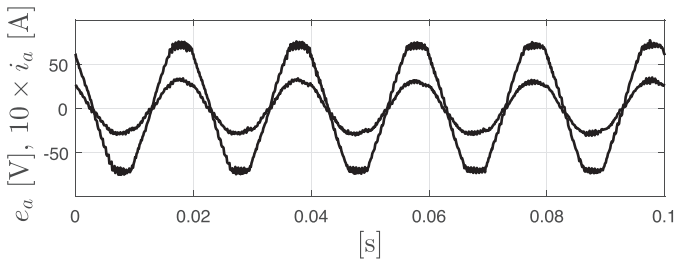
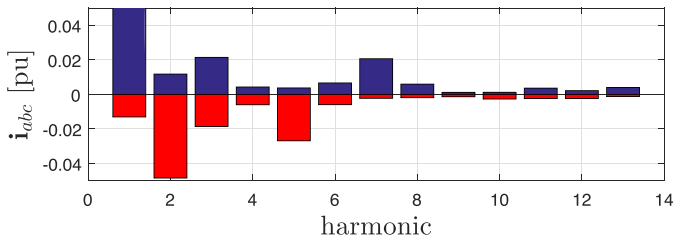**Fig. 10.** Current and voltage at phase *a* for a constant active power test (experimental results).

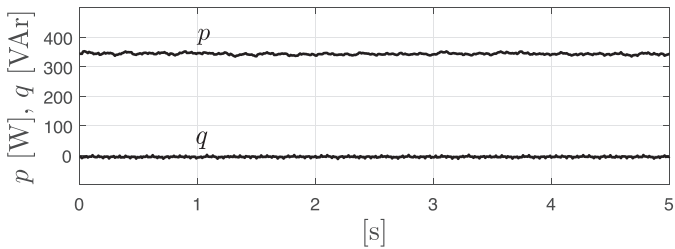**Fig. 11.** Frequency spectrum of grid current at phase *a* for a constant active power test (experimental result).

Fig. 12. Average active and reactive powers for a constant active power test (experimental results).

Fig. 13. Current and voltage at phase *a* for a change in reactive reactive power setpoint (experimental results).

Fig. 14. Average active and reactive powers for a change in reactive reactive power setpoint (experimental results).

Fig. 15. Input current for a change in the input power (experimental result).

Fig. 16. DC-link voltage for a change in the input power (experimental result).

active power to the grid without reactive power injection. The input power is 350 W and the reference voltage of the DC-link is set in 185 V. It can be observed in Fig. 10 that the current injected to the grid has a sinusoidal waveform and is also in phase with the voltage. It is worth mentioned that for our experimental setup, the low value of the available power could introduce additional distortion in the output current. Moreover, switches dead-times and other disturbances could have a more important effect in this case than for a higher power setup. However, as can be appreciated in the frequency spectrum of the current i_a shown in Fig. 11, the harmonic components of the injected current are kept within the values allowed by standard (below 5%).

The average value of the instantaneous active and reactive powers for the test described above is shown in Fig. 12. It can be observed that the active power has a constant average value of 350 W and reactive power remains close to zero, with a small error due to uncertainty in the parameters of the system, mainly in the RL filter values. In some cases, when RL parameters can have a significant variation with temperature, or the error introduced by this variation is unacceptable, the proposed controller can be extended by adding an integral action controller using the same IDA approach, as proposed in Serra et al. [8].

Fig. 13 shows voltage and current of phase *a* for a test that consists of changing the set-point of reactive power exchanged with the grid from 60 VAr to 0 VAr. It can be observed that the current injected into the grid is out of phase with the voltage during the first 50 ms. Starting from this time, output current is in phase with the grid voltage because the system stops injecting reactive power
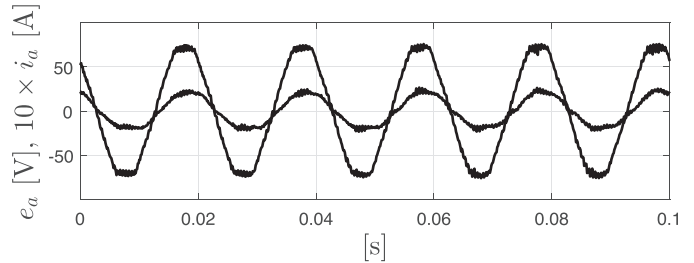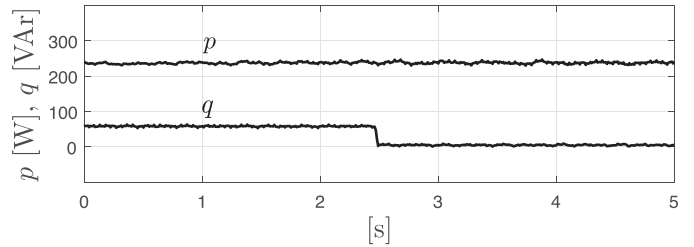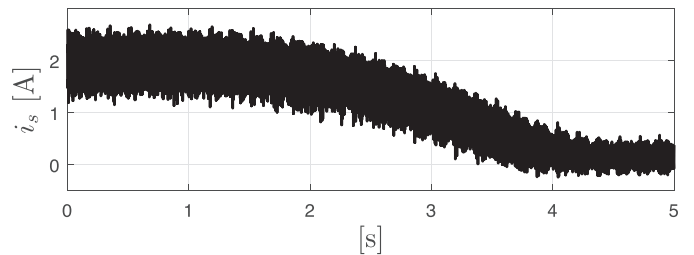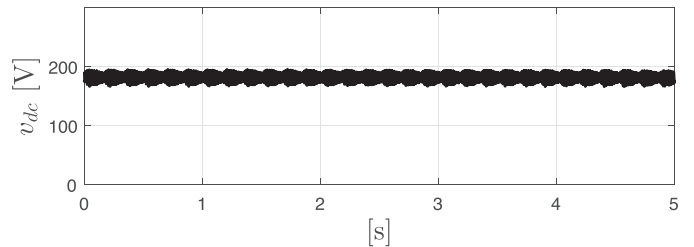
to the grid. It can be seen that, as in the previous test, the current injected into the grid has a sinusoidal waveform and is free of significant distortions. The instantaneous active and reactive powers for this test are shown in Fig. 14. As it can be appreciated, the proposed controller shows the advantage of an independent control of active and reactive powers, obtained from the decoupling between i_d and i_q currents.

To experimentally verify the performance of the control strategy to changes in the input power, a test was performed consisting on making a smooth change in the input power without reactive power injection. Fig. 15 shows the evolution of the input current, i_s, over 5 s while Fig. 16 shows the DC-link voltage. It can be observed that the proposed control strategy allows to regulate the voltage of the DC-link through Eq. (32). Despite the power change (reduction of i_s), voltage v_{dc} remains constant, demonstrating that the control strategy allows regulating v_{dc}. It must be noted that with the proposed controller, DC-link voltage regulation is obtained from the
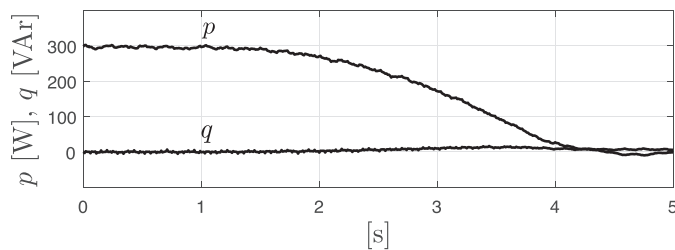
Fig. 17. Average active and reactive power for a change in the input power (experimental results).

same design methodology, without the need of designing an additional control loop as in previous proposals. Finally, Fig. 17 shows the average value of the instantaneous active and reactive powers for this test.

5. Discussion and conclusions

In this paper we presented the design of a controller for a FEC based on IDA, with the objectives of injecting all the available power on the DC side to the grid and controlling the reactive power exchanged with the power system, while ensuring that the current injected to the grid complies with international standards.

The proposal allows the injection of sinusoidal currents to the grid without the need for multi-loop controllers. It also takes into account both imbalance and harmonic content of the grid voltage and the distortion on the input current.

As it was demonstrated with this proposal, the IDA based design has the advantage of being a systematic design method in which determining the controller parameters results a simple task. This methodology allowed relating the state variables of the system in order to achieve direct control of the DC-link voltage using a reference equation for the direct axis current. That is, without the need of an additional voltage control loop as in previous works. Besides, independent control of the active and reactive power is obtained, due to the d and q axis currents decoupling stated from the design stage. Moreover, the obtained controller ensures asymptotic stability of the closed loop system.

The validation of the proposed control strategy was performed by simulation and experimental results. These results show that the system can inject all the power available at the DC side to the grid, being the injected currents sinusoidal, without significant distortions. Even when the experimental setup has a limited power, the measured current distortion is below the limits established by standards. It was also observed that the system controls the injected reactive power and the DC-link voltage remains at its reference value despite changes in the input power and control set-points.

Acknowledgements

References

[1] G. Tsengenes, G. Adamidis, Investigation of the behavior of a three phase grid-connected photovoltaic system to control active and reactive power, Electric Power Syst. Res. 81 (1) (2011) 177–184.
[2] S.I. Nanou, A.G. Papakonstantinou, S.A. Papathanassiou, A generic model of two-stage grid-connected PV systems with primary frequency response and inertia emulation, Electric Power Syst. Res. 127 (2015) 186–196.
[3] T.C. Green, M. Prodanovi, Control of inverter-based micro-grids, Electric Power Syst. Res. 77 (9) (2007) 1204–1213.
[4] M. Castilla, J. Miret, A. Camacho, J. Matas, L.G. de Vicuna, Reduction of current harmonic distortion in three-phase grid-connected photovoltaic inverters via resonant current control, IEEE Trans. Ind. Electron. 60 (4) (2013) 1464–1472.
[5] IEEE, Standard for Interconnecting Distributed Resources with Electric Power Systems, IEEE Standard, 2003, pp. 1547–2003.
[6] M. Chinchilla, S. Arnaltes, J.C. Burgos, Control of permanent-magnet generators applied to variable-speed wind-energy systems connected to the grid, IEEE Trans. Energy Convers. 21 (1) (2006) 130–135.
[7] J. de Matos, F. e Silva, L. Ribeiro, Power control in AC isolated microgrids with renewable energy sources and energy storage systems, IEEE Trans. Ind. Electron. 62 (6) (2015) 3490–3498.
[8] F.M. Serra, C.H. De Angelo, D.G. Forchetti, Interconnection and damping assignment control of a three-phase front end converter, Int. J. Electr. Power Energy Syst. 60 (2014) 317–324.
[9] S. Yang, Q. Lei, F.Z. Peng, Z. Qian, A robust control scheme for grid-connected voltage-source inverters, IEEE Trans. Ind. Electron. 58 (1) (2011) 202–212.
[10] A. Yazdani, R. Iravani, A unified dynamic model and control for the voltage-sourced converter under unbalanced grid conditions, IEEE Trans. Power Deliv. 21 (3) (2006) 1620–1629.
[11] Y.A.-R.I. Mohamed, E.F. El-Saadany, A control scheme for PWM voltage-source distributed-generation inverters for fast load-voltage regulation and effective mitigation of unbalanced voltage disturbances, IEEE Trans. Ind Electron 55 (5) (2008) 2072–2084.
[12] J. Eloy-Garcia, S. Arnaltes, J.L. Rodriguez-Amenedo, Direct power control of voltage source inverters with unbalanced grid voltages, IET Power Electron. 1 (3) (2008) 395–407.
[13] L. Shang, D. Sun, J. Hu, Sliding-mode-based direct power control of grid-connected voltage-sourced inverters under unbalanced network conditions, IET Power Electron. 4 (5) (2011) 395–407.
[14] L. Xiao, S. Huang, K. Lu, DC-bus voltage control of grid-connected voltage source converter by using space vector modulated direct power control under unbalanced network conditions, IET Power Electron. 6 (5) (2013) 395–407.
[15] T.H. Nguyen, D.C. Lee, Control strategy for three-phase grid-connected converters under unbalanced and distorted grid voltages using composite observers, J. Power Electron. 13 (3) (2013) 469–478.
[16] Q.-N. Trinh, H.-H. Lee, An enhanced grid current compensator for grid-connected distributed generation under nonlinear loads and grid voltage distortions, IEEE Trans. Ind. Electron. 61 (12) (2014) 6528–6537.
[17] J.I. Jang, D.C. Lee, High performance control of three-phase pwm converters under nonideal source voltage, IEEE Int. Conf. Ind. Technol. (ICIT) (2006) 2791–2796.
[18] J.H. Lee, H.G. Jeong, K.B. Lee, Performance improvement of grid-connected inverter systems under unbalanced and distorted grid voltage by using a PR controller, J. Electr. Eng. Technol. 7 (6) (2012) 918–925.
[19] J. Hu, Y. He, L. Xu, D. Zhi, Predictive current control of grid-connected voltage source converters during network unbalance, IET Power Electron. 3 (5) (2010) 690–701.
[20] R. Ortega, A. van der Schaft, B. Maschke, G. Escobar, Interconnection and damping assignment passivity-based control of port-controlled hamiltonian systems, AUTOMATICA 38 (4) (2002) 585–596.
[21] R. Ortega, E. Garcia-Canseco, Interconnection and damping assignment passivity-based control: a survey, Eur. J. Control 10 (2004) 432–450.
[22] A. Doria-Cerezo, C. Batlle, G. Espinosa-Perez, Passivity-based control of a wound-rotor synchronous motor, IET Control Theory Appl. 4 (10) (2010) 2049–2057.
[23] F.M. Serra, D.G. Forchetti, C.H. De Angelo, Comparison of positive sequence detectors for shunt active filter control, in: IEEE Int. Conf. Ind. Appl. (INDUSCON), 2010, pp. 1–6.
[24] M.R. Curti, F.M. Serra, D.G. Forchetti, C.H. De Angelo, Experimental implementation of PSDs, in: IEEE Int. Conf. Ind. Appl. (INDUSCON), 2012, pp. 1–6.